JOURNAL OF VIROLOGY, Nov. 2001, p. 10880–10891 Vol. 75, No. 22
0022-538X/01/$04.00+0 DOI: 10.1128/JVI.75.22.10880–10891.2001

Caveolae Are Involved in the Trafficking of Mouse Polyomavirus Virions and Artificial VP1 Pseudocapsids toward Cell Nuclei

ZUZANA RICHTEROVÁ,[1] DAVID LIEBL,[1] MARTIN HORÁK,[1] ZDENA PALKOVÁ,[1] JITKA ŠTOKROVÁ,[2] PAVEL HOZÁK,[3,4] JAN KORB,[2] AND JITKA FORSTOVÁ[1]*

Departments of Genetics and Microbiology[1] and Cell and Molecular Biology,[4] Charles University, and Institute of Molecular Genetics[2] and Institute of Experimental Medicine, Department of Cell Ultrastructure and Molecular Biology,[3] Academy of Sciences of the Czech Republic, Prague, Czech Republic

Received 9 April 2001/Accepted 1 August 2001

Electron and confocal microscopy were used to observe the entry and the movement of polyomavirus virions and artificial virus-like particles (VP1 pseudocapsids) in mouse fibroblasts and epithelial cells. No visible differences in adsorption and internalization of virions and VP1 pseudocapsids ("empty" or containing DNA) were observed. Viral particles entered cells internalized in smooth monopinocytic vesicles, often in the proximity of larger, caveola-like invaginations. Both "empty" vesicles derived from caveolae and vesicles containing viral particles were stained with the anti-caveolin-1 antibody, and the two types of vesicles often fused in the cytoplasm. Colocalization of VP1 with caveolin-1 was observed during viral particle movement from the plasma membrane throughout the cytoplasm to the perinuclear area. Empty vesicles and vesicles with viral particles moved predominantly along microfilaments. Particle movement was accompanied by transient disorganization of actin stress fibers. Microfilaments decorated by the VP1 immunofluorescent signal could be seen as concentric curves, apparently along membrane structures that probably represent endoplasmic reticulum. Colocalization of VP1 with tubulin was mostly observed in areas close to the cell nuclei and on mitotic tubulin structures. By 3 h postinfection, a strong signal of the VP1 (but no viral particles) had accumulated in the proximity of nuclei, around the outer nuclear membrane. However, the vast majority of VP1 pseudocapsids did not enter the nuclei.

Structural proteins of nonenveloped viruses are selected by evolution for the efficient delivery of genetic information via plasma membranes into cells for its expression. Hence, studying the properties of viral coat structures and detailed understanding of early steps of viral infection (entry, movements toward the cell nuclei, and uncoating) could help to solve an important aspect of gene therapy: the development of efficient systems for the transfer of exogenous genetic information into target cells.

Polyomaviruses, a member of the *Papovaviridae* family, have a wide range of hosts and different pathogenic responses in infected organisms. Despite this variation, the structures of the virions and genomic organizations of these viruses are very similar. Genomic circular double-stranded DNA (5.3 kbp) of the mouse polyomavirus encodes three early antigens (large, middle, and small T antigen) and three late structural proteins, VP1, VP2, and VP3. The late proteins, together with viral DNA and cellular histones (except H1), are assembled into virions in the cell nuclei. Neither VP2 nor VP3 is required for assembly of the capsid-like structure, and their functions in the viral replicative cycle are still unclear. The multifunctional VP1 can self-assemble into capsid-like particles (VP1 pseudocapsids) and is responsible for interaction with the sialic acid of an as-yet-unknown receptor (15, 37). Moreover, it has a nonspecific DNA binding activity (23), suggesting a role in nucleocore assembly. The problem is that little is known about the mechanisms of virion entry, trafficking, nuclear targeting, and uncoating. While the mouse polyomavirus, the simian lymphotropic papovavirus, and both human polyomaviruses, BK virus and JC virus, utilize sialic acid moieties of protein receptors for virion attachment to the cell surface (15, 17, 37), another member of the *Polyomavirinae* subfamily, simian virus 40 (SV40), utilizes major histocompatibility complex (MHC) class I molecules and has no hemagglutination ability (4). It has been reported recently that JC virus enters glial cells by clathrin-dependent receptor-mediated endocytosis (30), while SV40 enters cells by means of caveolae (3, 24). Vesicles containing SV40 virions are targeted into structures of the endoplasmic reticulum (ER). The uncoating process of polyomaviruses is not understood, but it is believed to be carried out after virions have entered the cell nuclei (6, 14, 20, 42–44). Earlier studies have revealed that mouse polyomavirus virions and natural empty capsids have different fates in infected cells. While virions enter cells in smooth monopinocytic vesicles and migrate to the nucleus, clusters of empty capsids internalized in large vesicles are targeted for degradation (13, 20).

It has previously been demonstrated that polyomavirus capsid-like particles could be produced in insect cells from a recombinant baculovirus carrying the gene for the polyomavirus major capsid protein, VP1 (9, 22). Such particles were easily purified to homogeneity and used for in vitro encapsidation of heterologous DNA. DNA partially encapsidated by VP1 pseudocapsids could be delivered into mammalian (including human) cells (10, 36, 38). However, the efficiency of gene delivery by VP1 pseudocapsids, measured by successful gene expression, was very low compared with that of infectious polyomavirus virions.

* Corresponding author. Mailing address: Department of Genetics and Microbiology, Charles University, Viničná 5, 128 44 Prague 2, Czech Republic. Phone: 420 2 21953177. Fax: 420 2 21953286. E-mail: jitkaf@natur.cuni.cz.

To better understand the early steps of mouse polyomavirus infection and the reasons for different gene transfer efficiencies of VP1 pseudocapsids and virions, we observed the internalization, movements, and interactions of virions and artificial VP1 pseudocapsids in NIH 3T6 mouse fibroblasts and normal murine mammary gland (NMuMG) epithelial cells by electron and confocal microscopy. In these experiments, high multiplicities of infections were used, reflecting conditions of natural cell reinfection as well as gene delivery via capsid-like particles.

MATERIALS AND METHODS

Cell cultivations and virus infections. *Spodoptera frugiperda* cells (Sf9) were grown as monolayer cultures at 27°C in TNF-FH medium containing 10% fetal calf serum as described by Hink (16). A recombinant baculovirus containing the polyomavirus VP1 gene was used for infection of Sf9 cells (10 PFU per cell) (9, 39). Infected cells were harvested 72 h postinfection (p.i.). Swiss albino mouse cells (NIH 3T6), NMuMG cells, and monkey kidney epithelial cells (CV-1) were grown at 37°C in a 5% CO_2–air humidified incubator, using Dulbecco's modified Eagle's medium (DMEM) supplemented with 2 mM glutamine and 10% fetal calf serum. For virion preparation, infection of NIH 3T6 cells with polyomavirus (A2 strain) was performed at a multiplicity of infection of 0.1 PFU per cell. Infected cells were harvested 7 days p.i.

Preparations of polyomavirus and VP1 pseudocapsids. VP1 capsid-like particles were isolated from infected Sf9 cells by CsCl and sucrose gradient centrifugations as described previously (9). Briefly, insect cells, infected with recombinant baculovirus and harvested 72 h p.i., were suspended in B buffer (150 mM NaCl, 10 mM Tris-HCl [pH 7.4], 0.01 mM $CaCl_2$) and disrupted by sonication. Cell debris was removed by centrifugation (10 min, 10 000 × g), and viral particles were purified from the supernatant by CsCl gradient centrifugation. A peak of "empty" VP1 pseudocapsids (buoyant density [ρ] = 1.294 − 1.283 g/cm^3) and a peak of "full" VP1 pseudocapsids (ρ = 1.348 − 1.315 g/cm^3) were further purified separately through a sucrose gradient (10 to 40%) and repeated CsCl gradients. Homogeneous fractions of particles were concentrated by pelleting through a 10% sucrose cushion and resuspending in B buffer. Polyomavirus virions were isolated from NIH 3T6 cell lysates by the procedure of Türler and Beard (40).

Confocal microscopy of double-stained mouse cells. NIH 3T6 or NMuMG cells grown on coverslips were infected by polyomavirus virions or VP1 pseudocapsids (10^3 to 10^4 particles per cell) in 200 μl of DMEM for 1 h at 37°C, after which 1 ml of complete medium was added. Cells were fixed, at indicated times p.i., with 3% paraformaldehyde and 0.01% glutaraldehyde (for 30 min) and permeabilized with 0.5% Triton X-100 in phosphate-buffered saline (for 5 min). Reactions with antibodies were performed as described previously (9). VP1 was visualized by using a rabbit anti-polyomavirus virion serum (kindly provided by Michael Pawlita) followed by the Alexa Fluor 488-goat anti-rabbit immunoglobulin G (IgG) antibody (green; Molecular Probes) or by using a mouse anti-VP1 pseudocapsid polyclonal antibody (prepared in our laboratory) followed by the Alexa Fluor 594-goat anti-mouse IgG antibody (red; Molecular Probes). Actin was stained by phalloidin conjugated with rhodamine (red; Sigma). Tubulin was visualized by mouse anti-α- and anti-β-tubulin monoclonal antibodies (EXBIO, Prague, Czech Republic) and then by a Cy3-sheep anti-mouse IgG antibody (red; Sigma). Caveolin-1 was visualized by a rabbit anti-caveolin-1 polyclonal antibody (Santa Cruz Biotechnology, Inc.) followed by the Alexa Fluor 488-goat anti-rabbit IgG antibody. Nuclei were visualized by interaction of DNA with propidium iodide (red; Propidium Iodide Antifade Kit, catalog no. S 1370-6; Oncor). Cells on coverslips were mounted with the ProLong Antifade Kit (Molecular Probes). The immunofluorescence signal was detected by 0.5-μm sectioning with a TNS SP Leica confocal laser scanning microscope, followed by digital image processing with TCS NT Leica software.

Electron microscopy. NIH 3T6 or NMuMG cells grown on coverslips were infected with polyomavirus virions or VP1 pseudocapsids (10^4 to 10^5 particles per cell). At appropriate times p.i., cells were processed for transmission electron microscopy. Briefly, infected cells were washed in phosphate-buffered saline, fixed with 3% glutaraldehyde in 0.1 M cacodylate buffer, postfixed with 1% osmium tetroxide, dehydrated through an increasing ethanol series (including a 30-min incubation in 1.5% uranyl acetate in 70% ethanol), and flat-embedded in Agar 100 resin (Gröpl, Tulln, Austria). Sections (70 nm) were contrasted with a saturated uranyl acetate solution in water (10 min at room temperature[RT]), and Reynold's lead citrate (7 min at RT). Samples were observed with a JEOL JEM 1200EX electron microscope operating at 60 kV.

Immunoelectron microscopy. Cells were grown on coverslips and, after incubation with virus or VP1 pseudocapsids, were flat-embedded by the method of Lee et al. (19). In brief, cells were rinsed with Sörensen buffer (SB), fixed with 1% paraformaldehyde and 0.1% glutaraldehyde in SB, and permeabilized with 0.1% Triton X-100 in SB. After several washes in SB, cells were incubated (overnight, 4°C) with a rabbit anti-caveolin-1 polyclonal antibody alone or together with a mouse anti-VP1 pseudocapsid polyclonal antibody, both diluted in 1% Tween 20 in SB. This was followed by incubation (overnight, 4°C) with a goat anti-rabbit IgG antibody conjugated with 10- or 15-nm-diameter gold particles (British Biocell Int.), alone or mixed with a goat anti-mouse IgG antibody conjugated with 5-nm gold particles (British Biocell Int.), both diluted in 0.5% bovine serum albumin in SB. Cells were refixed with 2.5% glutaraldehyde and 2.0% paraformaldehyde in SB and postfixed with 0.5% osmium tetroxide in SB. Samples were dehydrated through an ascendant ethanol series, flat-embedded in Agar 100 resin, contrasted, and observed as described above.

Inhibition of infection. Mouse NIH 3T6 fibroblasts, NMuMG epithelial cells, and monkey CV-1 cells grown on coverslips were incubated in DMEM with addition of 0.1, 5, and 7.5 mM methyl-β-cyclodextrin, respectively, at 37°C for 1 h. Then the NIH 3T6 and NMuMG cells were incubated for 90 min with polyomavirus, and the CV-1 cells were incubated for 90 min with SV40 (both at 10 PFU per cell), still in the presence of the drug. Cells were washed three times with DMEM and incubated in a complete medium for 42 h (polyomavirus infected) or 48 h (SV40 infected) at 37°C. To control cells, transferrin (10 μg/ml) was added instead of the virus and cells were incubated for 30 min at 0°C, followed by a 30-min incubation at 37°C and repeated washing with cold DMEM. Cells were fixed as described above and visualized by indirect immunofluorescence using antibodies against the polyomavirus or SV40 VP1 antigen (kindly provided by Harumi Kasamatsu) or transferrin (EXBIO).

RESULTS

Preparation of viral particles. In addition to purified natural polyomavirus virions, we examined two types of VP1 pseudocapsids purified from insect cells infected with a recombinant baculovirus carrying the polyomavirus VP1 gene: (i) "empty" VP1 pseudocapsids, which had previously been shown to interact in vitro with naked DNA fragments, partially encapsidate them (up to 3 kbp), and deliver them for their expression into mammalian cells (36, 38) and (ii) "full" VP1 pseudocapsids, which had already encapsidated baculoviral and host DNA fragments of polyomavirus genome size (5 kbp), together with cell histones, inside the insect cells and did not bind DNA in vitro (12, 25, 28).

The purity of all types of particles was verified by Coomassie blue staining of sodium dodecyl sulfate-polyacrylamide gel electrophoresis (SDS-PAGE) gels and by Western blotting. Their comparison did not reveal any protein of non-VP1 origin on SDS-PAGE gels in preparations of empty VP1 pseudocapsids. A characteristic pattern of small cellular proteins was observed in full VP1 pseudocapsid preparations as well as in virion preparations in which additional VP2 and VP3 bands were present (data not shown). Electron microscopy also confirmed the homogeneity of particle preparations (Fig. 1). Concentrations of particles were estimated by protein content measurement and by hemagglutination.

Surprisingly, we have not seen any differences in adsorption, internalization, or movement between empty and full VP1 pseudocapsids, either by electron microscopy or by confocal microscopy. Thus, we continue to use the term "VP1 pseudocapsids" for both, we present figures only for empty VP1 pseudocapsids.

Adsorption and internalization of virions and VP1 pseudocapsids. We examined the movement of viral particles in two cell lines, mouse NIH 3T6 fibroblasts and NMuMG epithelial cells. During the first step of infection, all three types of par-

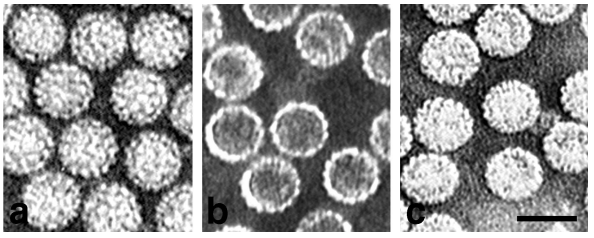

FIG. 1. Purified virions (a), empty VP1 pseudocapsids (b), and full VP1 pseudocapsids (c), visualized by electron microscopy (negative staining). Bar, 50 nm.

ticles were found adsorbed nonrandomly on certain cell surface areas (see Fig. 5Aa to Ac and Ba, 8a, and 9Aa and Ba). Particles exhibited a strong affinity for areas with high actin content, e.g., filopodia (Fig. 2). In contrast to earlier observations (14, 20), results of ultrastructural analysis revealed that not only virions (Fig. 3Aa, Ab, Ag, Ah, Ba, and Bb) but also VP1 pseudocapsids (Fig. 3Ad to Af and Ai) enter cells through smooth, non-clathrin-coated monopinocytic vesicles. In addition, an intensive formation of invaginations without viral particles was observed in areas of particle adsorption. The flask shape of invaginations was typical of caveolae. Similar areas with many invaginations were also found, although less frequently, in the control, mock-infected, cells (not shown). While caveola-like invaginations were 70 to 100 nm in diameter, invaginations containing particles were substantially smaller (approximately 60 nm in diameter), each one tightly enveloping the particle.

Colocalization of vesicles containing virions or VP1 pseudocapsids with caveolin-1. To elucidate whether empty caveola-like invaginations and/or vesicles containing particles colocalize with caveolin-1, we performed immunoelectron microscopy using the anti-caveolin-1 antibody (10- or 15-nm gold) (Fig. 4A and B). In some experiments, double staining with anti caveolin-1 and anti-VP1 (5-nm gold) was performed (Fig. 4C). Figure 4 clearly demonstrates that the caveola-like invaginations and empty vesicles often observed in the area of viral particle adsorption contain caveolin. Also, the invaginations and monopinocytic vesicles containing virions or VP1 pseudocapsids were labeled with the anti-caveolin-1 antibody. Early fusion of empty, caveolin-rich vesicles with monopinocytic vesicles carrying particles resulted in the formation of larger vesicles with two or more viral particles.

The colocalization of caveolin-1 with VP1 was also followed by confocal microscopy after double staining, using anti-VP1 (red) and anti-caveolin-1 (green) antibodies (Fig. 5). In both fibroblasts and epithelial cells, colocalization of caveolin-1 and VP1 was observed. Soon after adsorption, we observed preferential accumulation of caveolin in the membrane areas, where viral particles entered cells (Fig. 5Aa to Ac, Am, and Ba). In noninfected cells, strong accumulation of caveolin in the proximity of cell membrane was significantly less frequent (data not shown). In the cytoplasm, caveolin accompanied VP1 in its movement toward the cell nucleus (Fig. 5Ad to Ar, Bb, and Bc). The movement seemed to be realized along cytoskeletal filaments (Fig. 5Ag to Ai, An, and Ao). These results suggest that (i) polyomavirus and VP1 pseudocapsids do not enter cells through clathrin-coated pits, but rather in vesicles which are derived from caveolar domains or from membrane domains in close proximity to caveolae and (ii) empty vesicles derived from caveolae often fuse with particle-containing monopinocytic vesicles and might be involved in particle movement toward the cell nucleus.

Inhibition of polyomavirus infectivity by methyl-β-cyclodextrin. Lipid rafts, sphingolipid- and cholesterol-rich microdomains of the plasma membrane, are assumed to play a role in the transport of proteins in endocytic pathways (34). We examined whether cholesterol depletion by methyl-β-cyclodextrin affects polyomavirus infectivity. The SV40 virions which were shown to utilize caveolae for internalization (3) were tested for comparison. The ratio of infected to noninfected cells was scored by indirect immunofluorescence (Table 1). Each value was calculated from at least 800 cells (10 microscope optical fields) for polyomavirus and from at least 200 cells for SV40. The infectivity of both polyomavirus and SV40 decreased with increasing concentrations of methyl-β-cyclo-

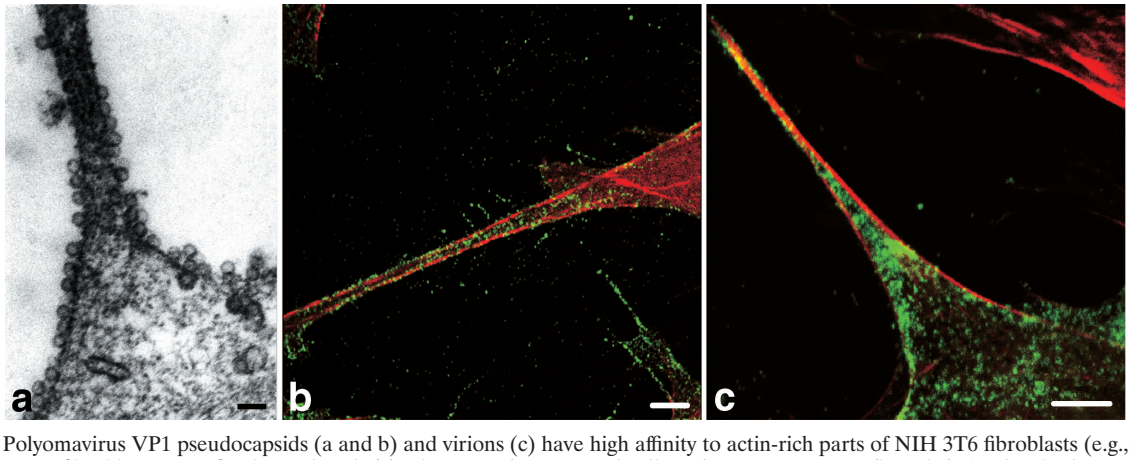

FIG. 2. Polyomavirus VP1 pseudocapsids (a and b) and virions (c) have high affinity to actin-rich parts of NIH 3T6 fibroblasts (e.g., filopodia). Mouse NIH 3T6 fibroblasts were fixed 20 min p.i. (a) Electron microscopy of cell section. Bar, 100 nm. (b and c) Confocal microscopy of cells stained with a rabbit anti-polyomavirus virion serum followed by the Alexa Fluor 488-goat anti-rabbit IgG antibody (green) and with phalloidin conjugated to rhodamine (red). Bars, 5 μm.

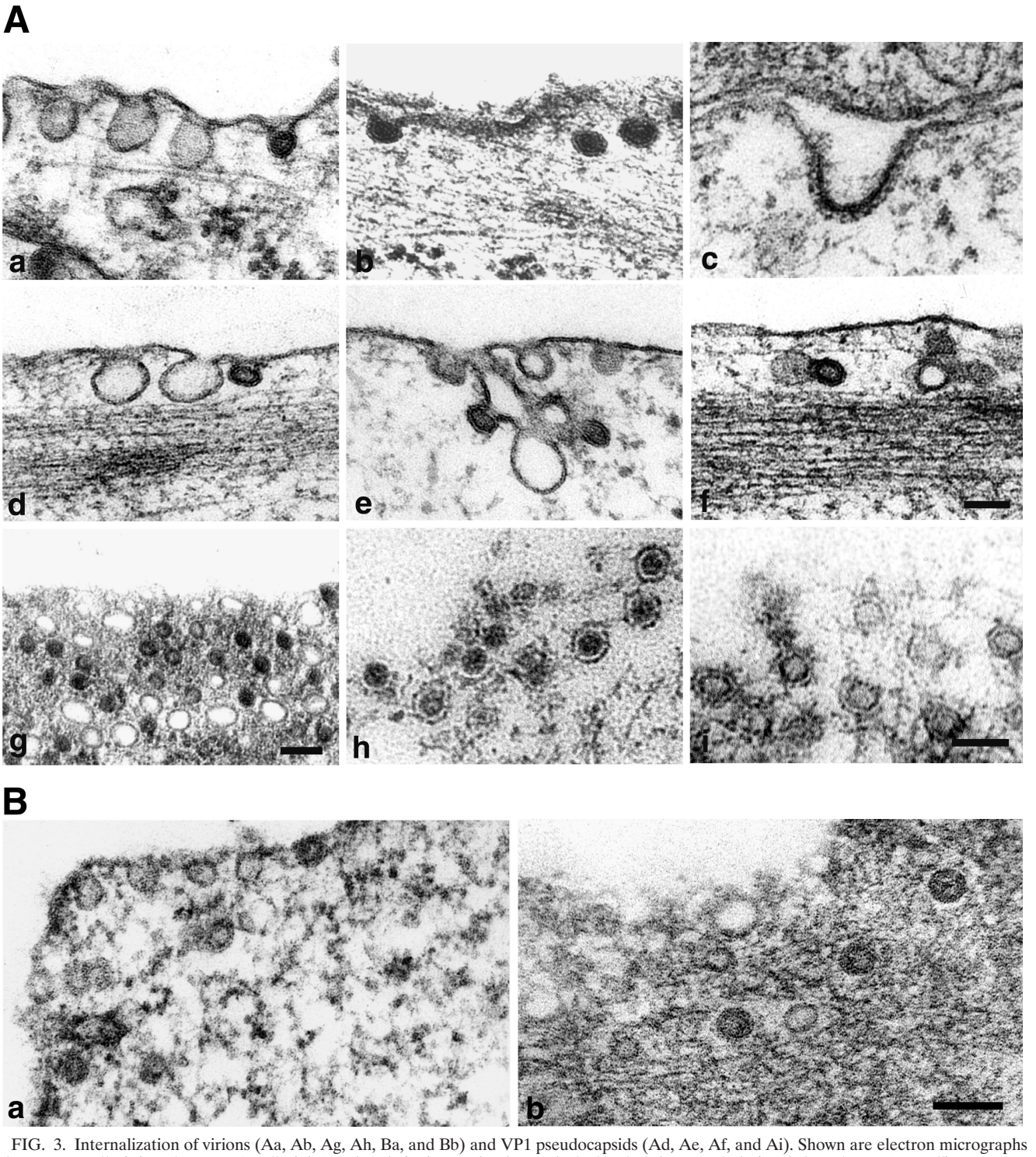

FIG. 3. Internalization of virions (Aa, Ab, Ag, Ah, Ba, and Bb) and VP1 pseudocapsids (Ad, Ae, Af, and Ai). Shown are electron micrographs of NIH 3T6 cells (A) and NMuMG cells (B) 20 min p.i. (Ac) Invagination typical of a clathrin-coated pit (noninfected NIH 3T6 cell). Bars, 100 nm.

dextrin. Treatment of cells with 5 mM methyl-β-cyclodextrin caused approximately 85% reduction of polyomavirus infection in both NIH 3T6 fibroblasts and NMuMG epithelial cells and 66% reduction of SV40 infection in CV-1 cells. Uptake of transferrin, which is internalized by clathrin-coated vesicles, was not significantly affected when NIH 3T6 fibroblasts and NMuMG epithelial cells were treated with 5 mM methyl-β-cyclodextrin (estimated by confocal microscopy; data not shown). These results indicate the importance of the presence of cholesterol for the endocytosis of polyomavirus, and they

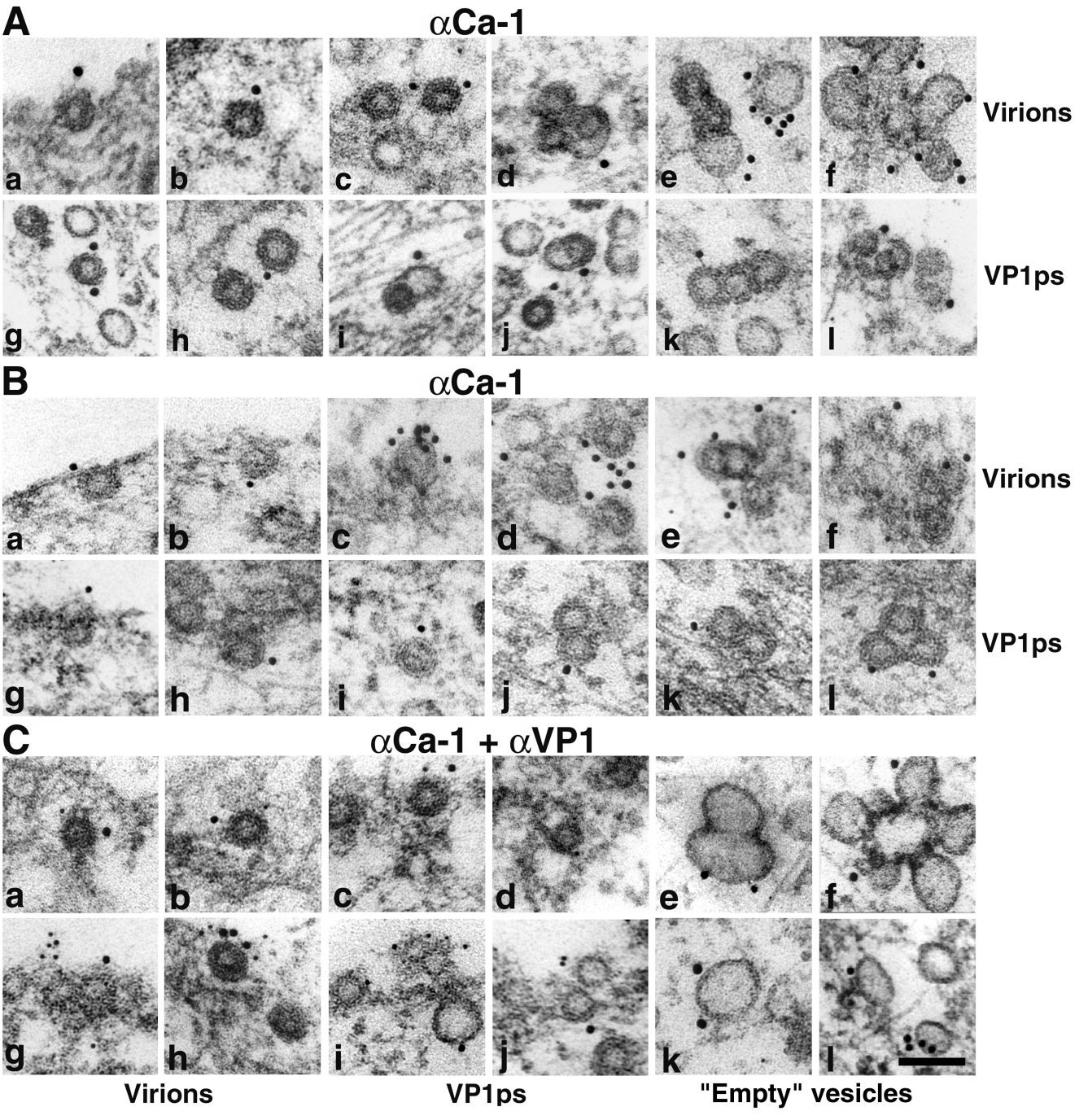

FIG. 4. Colocalization of invaginations and vesicles containing viral particles with caveolin-1. NIH 3T6 cells (A and Ca to Cf) and NMuMG cells (B and Cg to Cl) visualized by immunoelectron microscopy are shown at 20 min p.i. with virions or VP1 pseudocapsids (VP1ps). Note empty vesicles derived from caveolae (Ce, Cf, Ck, and Cl). (A and B) Staining with the rabbit anti-caveolin-1 polyclonal antibody followed by the 10- or 15-nm gold-goat anti-rabbit IgG antibody. (C) Double staining with the mouse anti-VP1 pseudocapsid polyclonal antibody followed by the 5-nm gold-goat anti-mouse IgG antibody and the rabbit anti-caveolin-1 polyclonal antibody followed by the 10- or 15-nm gold-goat anti-rabbit IgG antibody. Bar, 100 nm.

support the idea that polyomavirus enters cells, similarly to SV40, through cholesterol-rich lipid rafts.

Role of actin in vesicle movement. By ultrastructural analysis of cells harvested 20 min p.i., many virions and VP1 pseudocapsids, enveloped in monopinocytic vesicles, were found under plasma membranes. They were often aligned, in a similar manner to the caveola-derived empty vesicles, along the microfilament bundles (Fig. 6). The observed fusions of both types of vesicles were also most frequently found in these cell areas (Fig. 6c and d). Occasionally, particle-carrying vesicles, fusing with larger membrane structures, including ER, were detected (Fig. 7). Even at later times p.i., we have only rarely

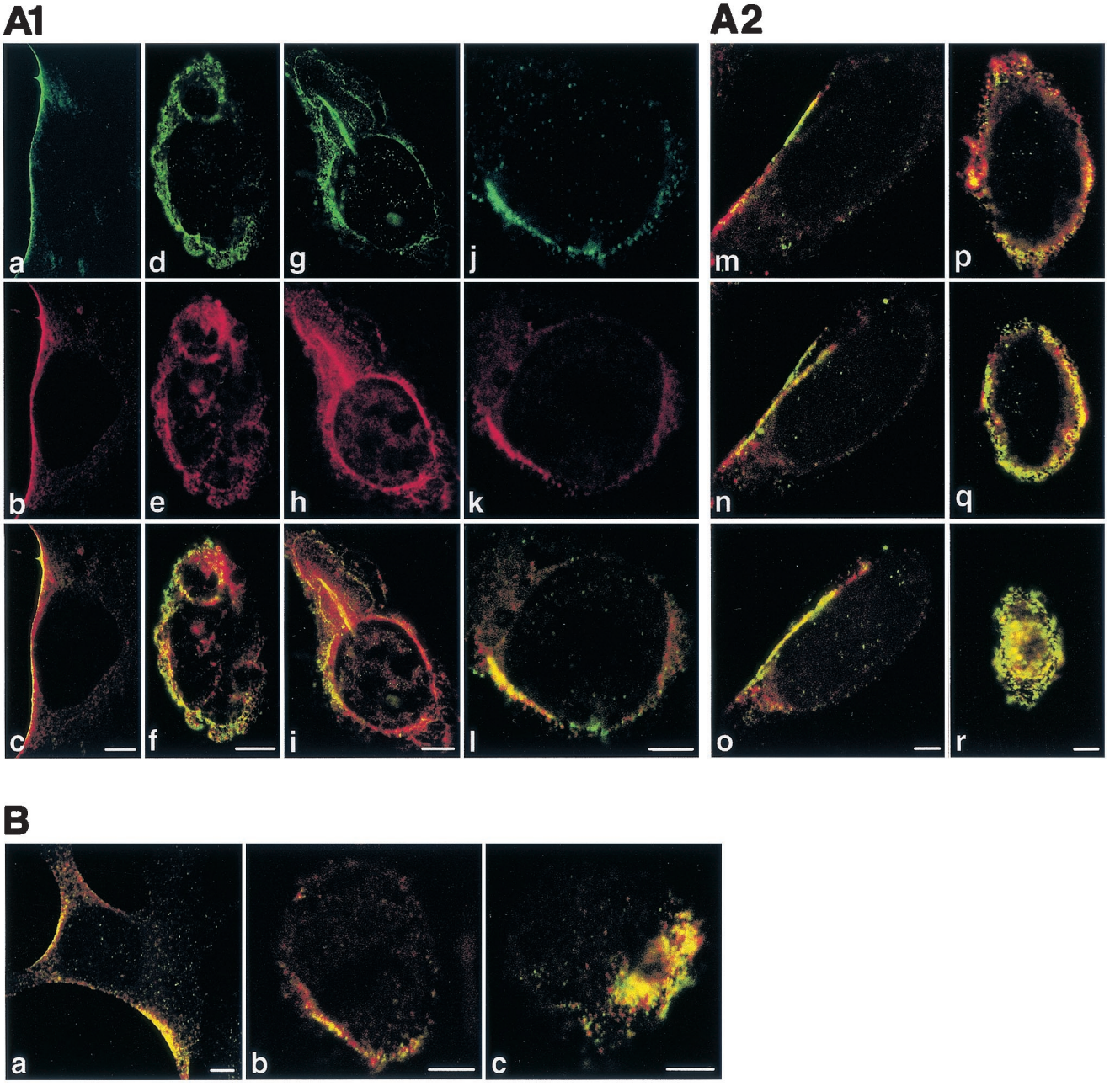

FIG. 5. Colocalization of caveolin-1 with VP1. NIH 3T6 (A) and NMuMG (B) cells visualized by confocal microscopy are shown at 20 min p.i. (Aa to Af and Ba) or 3 h p.i. (Ag to Ar, Bb, and Bc) with virions (A1 and B) and VP1 pseudocapsids (A2). (A1) Sections of cells. First row (a, d, g, and j), caveolin-1; second row (b, e, h, and k),VP1; third row (c, f, i, and l), merge. (A2) Merged section series of two cells (m, n, o and p, q, r). (B) Merged sections of three cells (a, b, c). Staining was performed with the mouse anti-VP1 pseudocapsid polyclonal antibody followed by the Alexa Fluor 594-goat anti-mouse IgG antibody (red) and with the rabbit anti-caveolin-1 polyclonal antibody followed by the Alexa Fluor 488-goat anti-rabbit IgG antibody (green). Bars, 5 μm.

observed particle-containing monopinocytic vesicles below the wall of actin filaments. Vesicles carrying particles that did not encounter the actin wall were found deeper in the cell interior. However, only in exceptional cases did we find a monopinocytic vesicle containing a distinct viral particle in close proximity to the nuclear membrane, and we have never seen the incoming intact virions or pseudocapsids entering the cell nucleus.

We also examined the colocalization of VP1 of pseudocapsids and virions with actin by confocal microscopy. In mock-infected cells, long, straight-lined actin stress fibers spanned most of the width of the cells (Fig. 8e). In the interval between 20 and 180 min p.i., most of the actin stress fibers disappeared, and disarranged actin microfilaments (red) decorated by VP1 (green) were observed as concentric curves around the cell-nucleus (Fig. 8b, c, f, and g). (A similar pattern of VP1 together with caveolin was observed in some cells [Fig. 5Ad to Ai]).

TABLE 1. Influence of methyl-β-cyclodextrin on polyomavirus and SV40 infectivity[a]

Methyl-β-cyclodextrin concn (mM)	% Infected cells[b]					
	Polyomavirus				SV40, in CV-1 cells	
	NIH 3T6 cells		NMuMG cells			
	Avg	Relative to control	Avg	Relative to control	Avg	Relative to control
0	43.09	100.00	48.63	100.00	62.11	100.00
1	24.97	57.95	23.99	49.33	44.44	71.55
5	6.57	15.25	7.00	14.39	21.30	34.29
7.5	6.48	15.04	6.45	13.26	20.65	33.25

[a] Infected cells were visualized by staining with antibodies against the VP1 antigen of polyomavirus or SV40.
[b] Avg, average percent infected cells from 10 optical fields. Relative to control, infected cells as a percentage of the number of infected cells present in the non-inhibitor-treated control sample.

Actin also appeared inside the cell nucleus. At later stages p.i. (3 h and more), when most of the VP1 reached areas near the cell nucleus, actin stress fibers were restored (Fig. 8d and h). The character of the VP1 signal of virions differed from that of pseudocapsids. While the virion signal was concentrated into distinct bright points, the pseudocapsid signal was stronger and was reminiscent of an amorphous, disassembled mass (Fig. 8c and d versus g and h).

Colocalization of VP1 with tubulin. At early times postadsorption (20 min), the VP1 signal was only occasionally seen

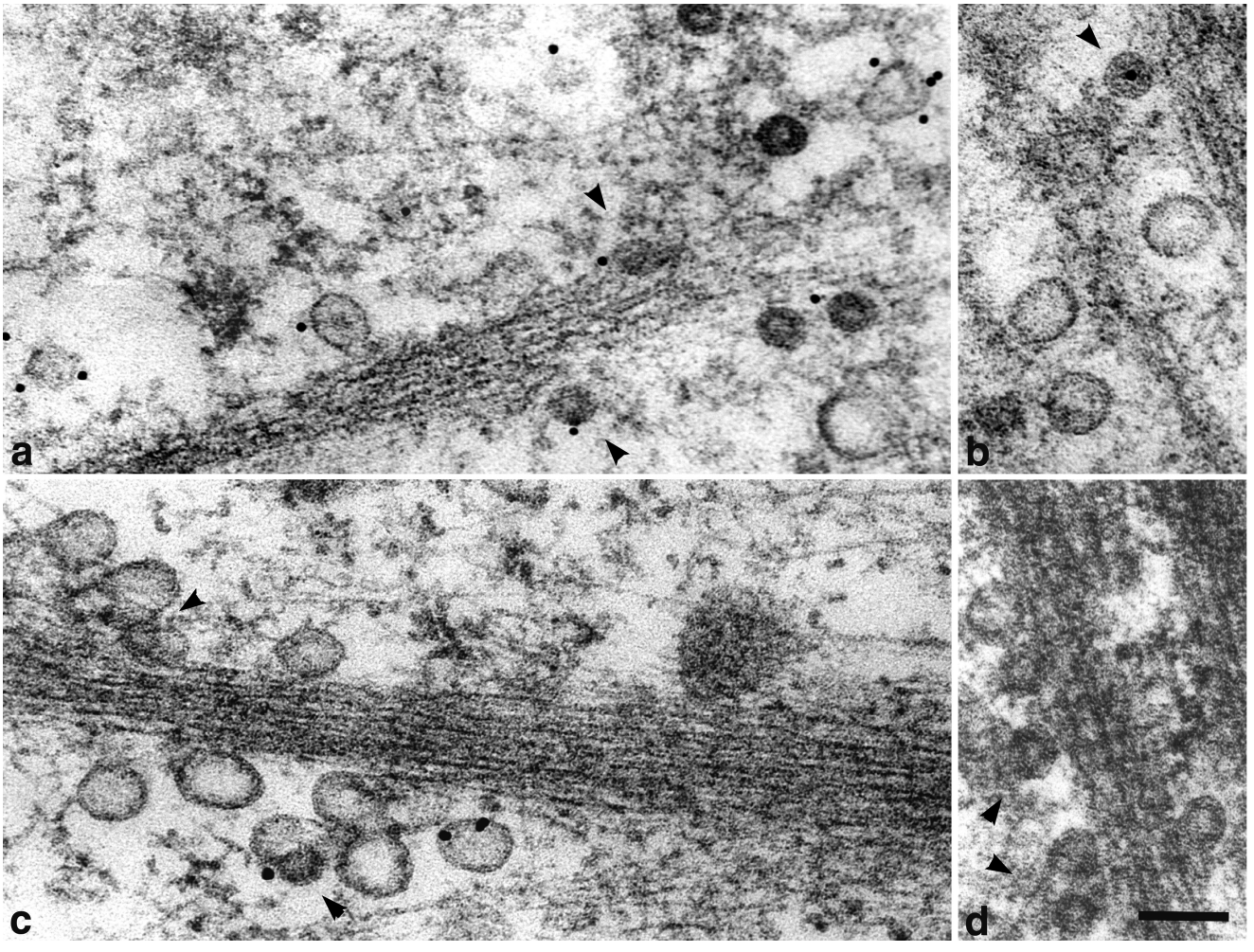

FIG. 6. Movement of vesicles containing virions (a and b) or VP1 pseudocapsids (c and d) and empty vesicles derived from caveolae along actin filaments in NIH 3T6 fibroblasts. Cell sections were visualized by electron and immunoelectron microscopy. Staining was done with the rabbit anti-caveolin-1 polyclonal antibody followed by the 10-nm gold-goat anti-rabbit IgG antibody. Arrowheads point to vesicles containing viral particles. Bars, 100 nm.

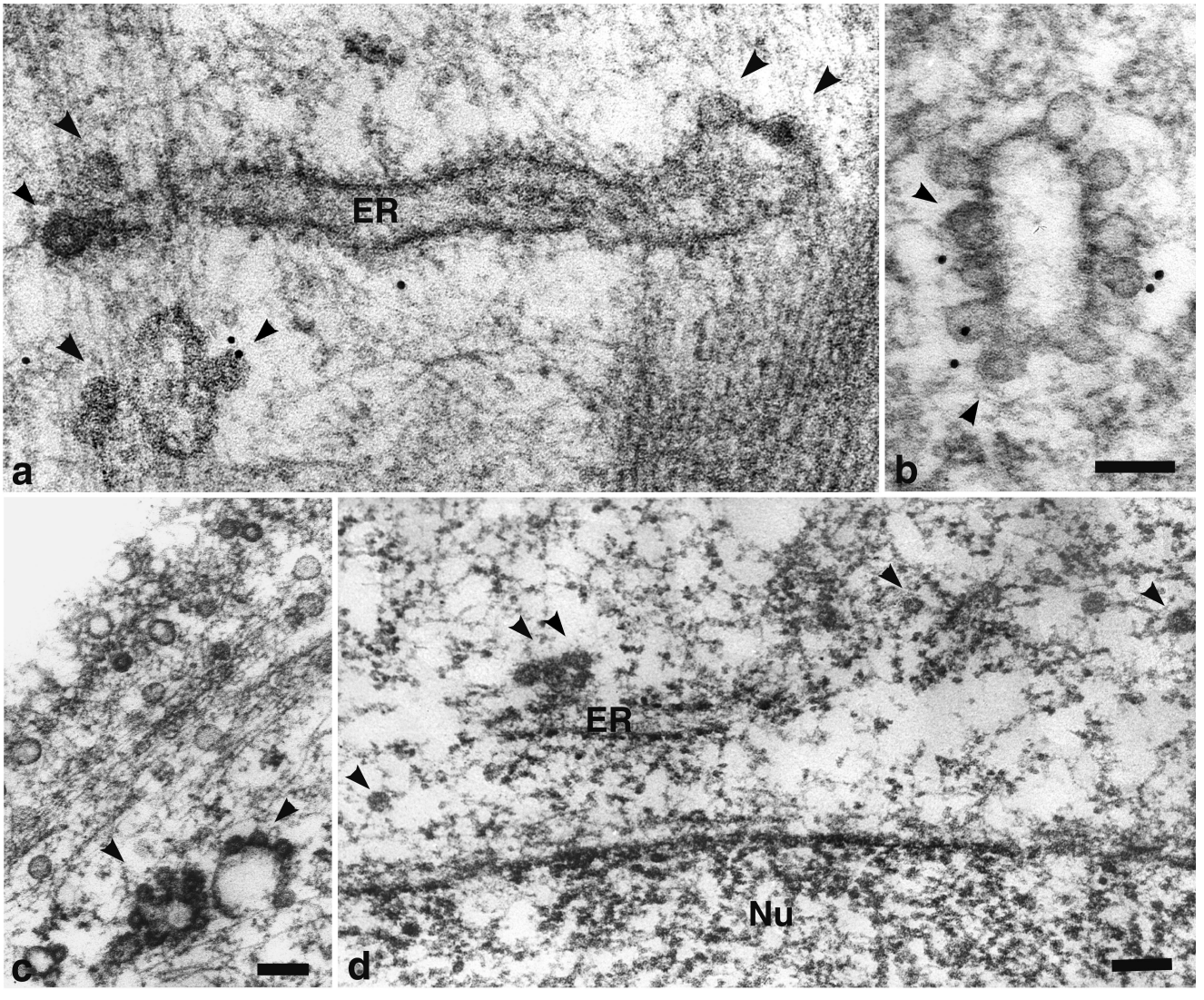

FIG. 7. Fusion of vesicles carrying viral particles with large membrane structures. NIH 3T6 cells infected with virions (a, b, and c) and NMuMG cells "infected" with VP1 pseudocapsids (d) were visualized by electron and immunoelectron microscopy. Staining was done with the rabbit anti-caveolin-1 polyclonal antibody followed by the 10-nm gold-goat anti-rabbit IgG antibody. Arrowheads point to fusing vesicles carrying viral particles. Nu, nucleus. Bars, 100 nm.

along microtubules (Fig. 9Aa and Ba). Later, more-frequent association of VP1 with microtubules was observed near the cell nucleus (Fig. 9Ab, Ac, Ae, Af, Bb, and Bc). Substantial colocalization of VP1 with tubulin was detected around nuclei (Fig. 9Ab and Ag) and on mitotic centromeres and spindles (Fig. 9Ad, Ah, and Bd). Because we have only occasionally seen vesicles with viral particles close to the nuclear membrane, we presume that observed colocalization might reflect either an association of larger membrane structures (containing VP1) with microtubules or a direct interaction of disassembled VP1 with microtubule structures.

The vast majority of VP1 from incoming virions and VP1 pseudocapsids does not enter the cell nucleus. As demonstrated by the confocal microscope sectioning, most VP1 accumulated around the outer nuclear membrane, bound to cytoskeletal structures and/or at the ER (Fig. 9Ab, Ac, and Ag). At 3 h p.i., no nuclear localization of the VP1 signal of either virions or VP1 pseudocapsids was detected in sections passing through the nucleus interior (Fig. 10a, b, d, and e). The distance between DNA stained with propidium iodide (red) and VP1 signal (green) (Fig. 10b and e) suggests the presence of an "interstructure," very probably the nuclear membrane. A cell section cut through the center of the nucleus (Fig. 10b) and sections showing the surface of the cell nucleus (Fig. 10c and f) demonstrate that VP1 is located around the cell nucleus in distinct points.

DISCUSSION

In this paper, we studied early steps of mouse polyomavirus infection, monitoring adsorption, internalization, and movements of viral particles in mouse NIH 3T6 fibroblasts and NMuMG epithelial cells. We also addressed the question whether any differences between virions and artificial VP1 pseudocapsids can be revealed.

Various nonenveloped DNA viruses, such as adenoviruses

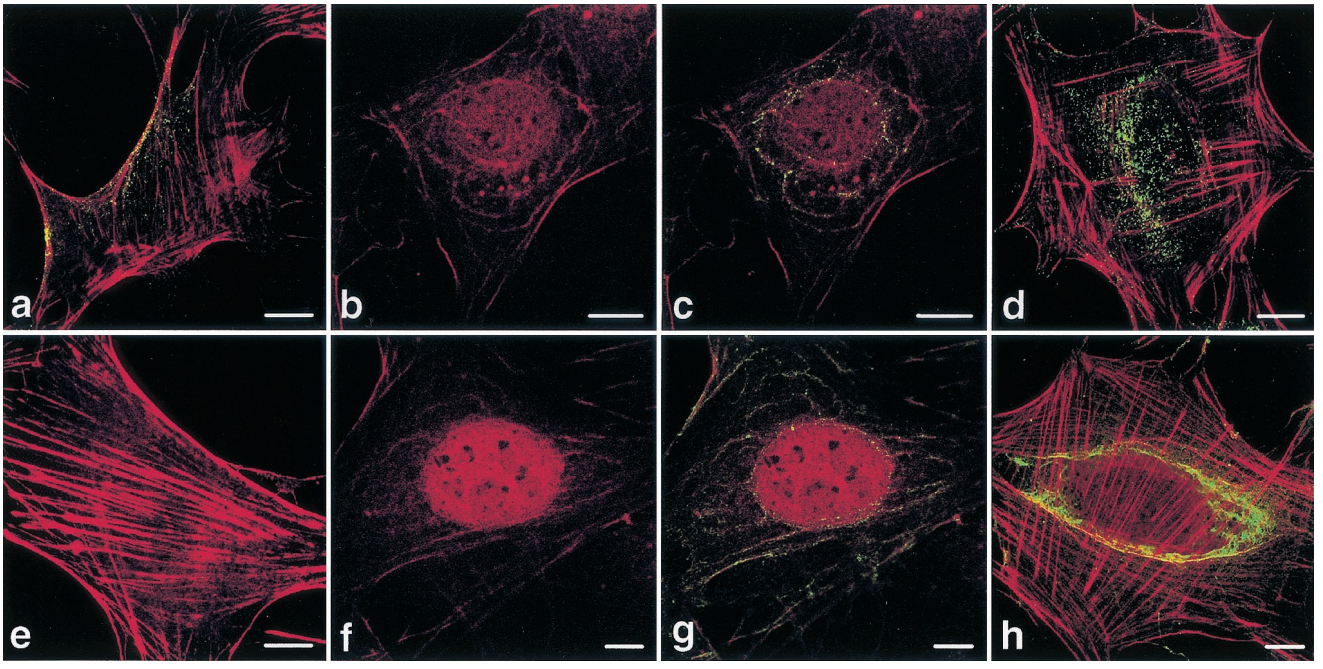

FIG. 8. Colocalization of actin with VP1 of virions (a to d) and pseudocapsids (f to h). Sections of NIH 3T6 cells fixed 20 min p.i. (a to c, f, and g) or 3 h p.i. (d and h) were visualized by confocal microscopy. (e) Control, mock-infected, cell fixed 20 min p.i. Staining was done with the rabbit anti-polyomavirus virion serum followed by the Alexa Fluor 488-goat anti-rabbit IgG antibody (green) and with phalloidin conjugated with rhodamine (red). Bars, 10 μm.

or adeno-associated viruses, enter cells by receptor-mediated endocytosis in clathrin-coated vesicles (5, 27, 41). The human polyomavirus JC virus, which recognizes a sialized receptor, has also been described entering cells in clathrin-coated pits (30), while SV40 is known to use caveolae for internalization (24). Although mouse polyomavirus also has an affinity to a sialized receptor, it becomes internalized in smooth, non-clathrin-coated monopinocytic vesicles. Invaginations around polyomaviruses were smaller than typical caveolae and were morphologically very similar to those around SV40 virions (24). As with SV40, we observed polyomavirus particles in multilobed, surface-connected invaginations, which have been described as characteristic of caveolae in many different cell types (26). Monopinocytic vesicles carrying all three types of particles examined interacted with the anti-caveolin-1 antibody, suggesting that they were derived either directly from caveolar domains or from lipid rafts located in close proximity to caveolae. Strong colocalization of VP1 with caveolin on cell membranes and the frequent appearance of caveolae in areas of viral particle adsorption suggest a high affinity of viral particles for caveolar domains and also the actual cumulation of caveolin induced by particle adsorption.

Both the association of vesicles containing particles with actin microfilaments and the reorganization of actin cytoskeleton after particle adsorption strongly support the role of rafts in viral particle internalization. It is known that cholesterol-rich rafts are concentrated in actin-rich regions of quiescent fibroblasts. In these domains, glycosylphosphatidylinositol-anchored proteins, transmembrane proteins, and double-acylated proteins, including small GTPases regulating actin cytoskeleton rearrangement, are concentrated (21, 35). In the membrane dynamic system, raft domains cluster together after ligand-receptor binding, thus enhancing signals transduced into a cell (35). Interactions of viral particles with rafts may induce similar processes, including signal transduction. This is also supported by earlier observations of increased c-*fos* and c-*myc* mRNA levels shortly after polyomavirus adsorption (46).

The role of cytoskeleton in polyomavirus trafficking is not yet clear. At early times p.i., when actin stress fibers temporarily disappeared, microfilaments aligned with VP1 signal were seen as concentric curves, decorating membranes around the nucleus, suggesting that microfilaments guide VP1 to the proximity of the ER (and/or possibly the Golgi apparatus). Detection of actin in the nucleus is in agreement with recent observations of the presence of actin and actin-binding proteins in the nucleus, e.g., under stress conditions (31). Later (3 h p.i.), when the majority of the VP1 signal appeared around the cell nucleus, stress fibers recovered.

Alignment of VP1 signal with microtubules was only rarely seen in the earliest stages of infection. A higher extent of VP1-tubulin association was found later (3 h p.i.), when the VP1 label appeared closer to the nucleus. However, in these areas of cells, no free viral particles and only a few monopinocytic vesicles containing viral particles were found. Therefore, the alignment of VP1 and tubulin signals represents the trafficking of particle-containing monopinocytic vesicles and/or the transport of larger endosomes (created by fusions of monopinocytic vesicles with caveola-derived vesicles), in which viral particles might be partially disassembled. The colocalization of VP1 with tubulin around the nucleus could reflect an alignment of microtubules with ER structures, where the VP1 of a majority of incoming viral particles seems to accumulate.

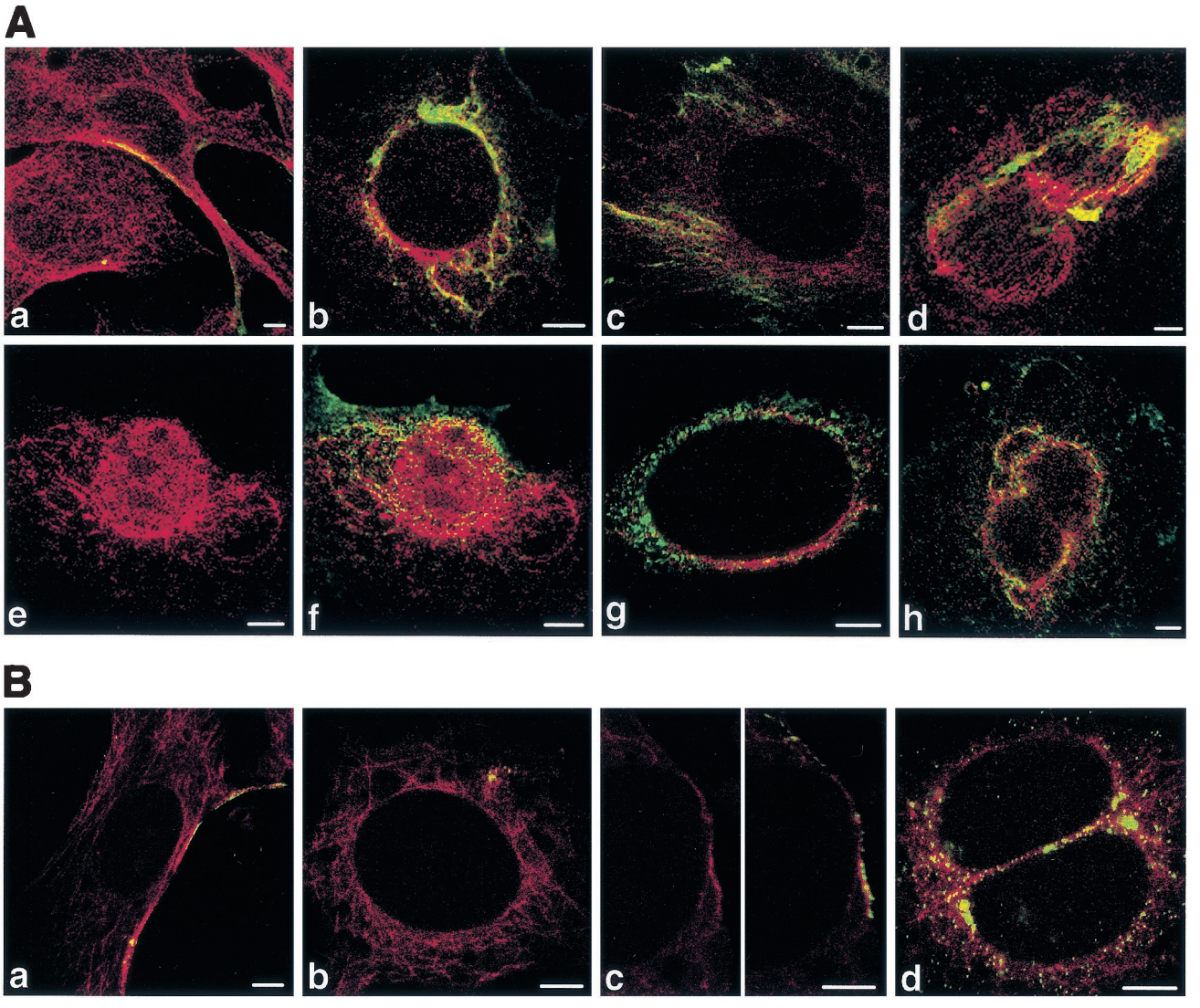

FIG. 9. Colocalizations of tubulin with VP1 of pseudocapsids (Aa to Ad) and virions (Ae to Ah and B). Sections of NIH 3T6 fibroblasts (A) and NMuMG (B) cells fixed 20 min p.i. (Aa and Ba) or 3 h p.i. (Ab to Ah and Bb to Bd) were visualized by confocal microscopy. Staining was done with the rabbit anti-polyomavirus virion serum followed by the Alexa Fluor 488-goat anti-rabbit IgG antibody (green) and with the mouse anti-α- and anti-β-tubulin antibody followed by the Cy3-sheep anti-mouse IgG antibody (red). Bars: 5 μm.

Strong colocalization of mitotic tubulin structures with VP1 is probably mediated by the vesicular membranous structures, derived from ER, which are known to be located along the mitotic spindle during mitosis. Nor can we rule out a direct interaction of mitotic tubulin structures with disassembled VP1, released from ER. Interaction of newly synthesized VP1 with mitotic spindle structures was evidenced during VP1 production in yeast cells (25).

Thus, actin appears to play a role in early stages of virus movement, while microtubules play a role in later stages. However, in the recent experiments of Krauzewicz et al. (18), a microfilament-destroying agent, cytochalasin D, had no effect either on polyomavirus infectivity or on the expression level of genes delivered by VP1 pseudocapsids, while the microtubule-disrupting agent nocodazole inhibited both efficiently. This suggests the hypothesis of two trafficking routes, only one of which results in productive targeting of virions. In the case of polyomavirus, actin bundles might function as a protective wall of filaments, which leads vesicles with particles to dock in compartments where they are doomed to degradation. On the other hand, microtubules could direct vesicles with particles to the proper targets, thus enabling the delivery of viral information into the cell nucleus. The sensitivity of viral infection to microtubule-destroying agents was also observed for SV40 (33), while papillomavirus infection is abolished by both microfilament- and microtubule-disrupting chemicals (45).

While this report was under review, a paper describing a new, two-step vesicular-transport pathway to the ER, revealed by studies of caveolar endocytosis of SV40, was published (29). Using video-enhanced, live fluorescence microscopy, the authors showed that monopinocytic vesicles with SV40 enter larger, peripheral organelles, rich in caveolin-1, which they named caveosomes. In these nonacidic organelles, SV40 is sorted into tubular, caveolin-free membrane vesicles that move

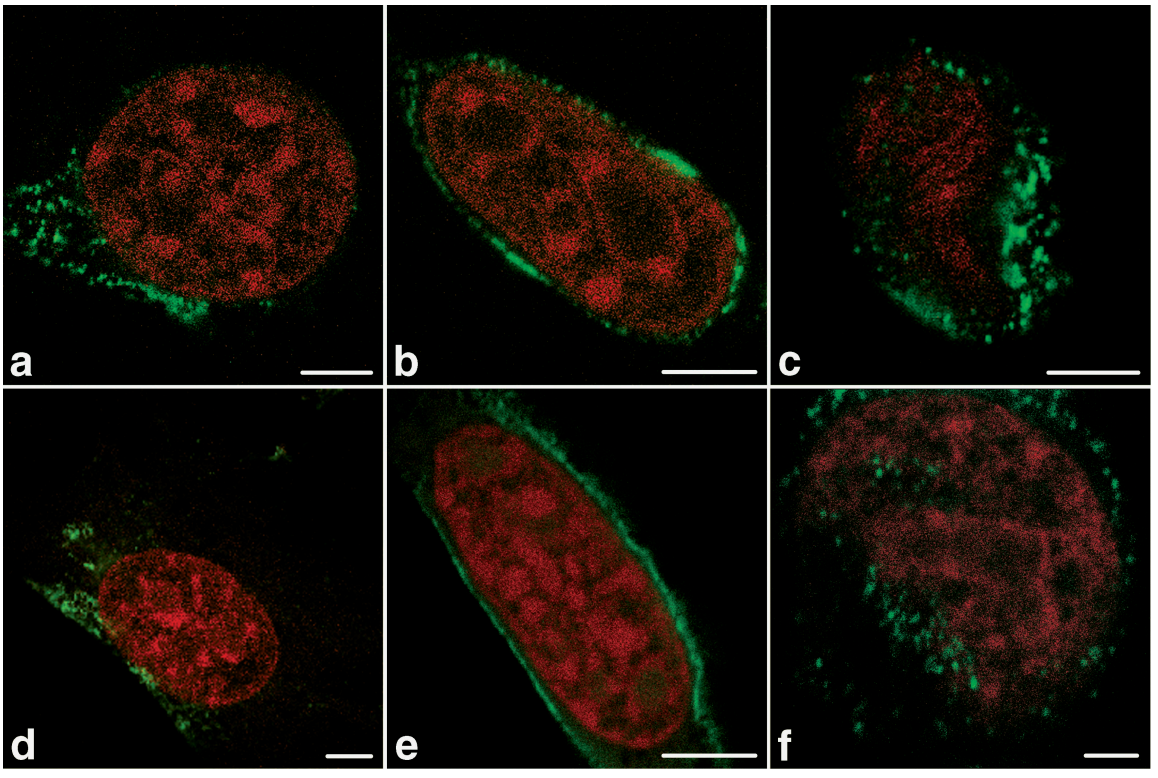

FIG. 10. The majority of VP1 of incoming virions (a to c) and pseudocapsids (d to f) does not enter the cell nucleus. Sections of 3T6 cells fixed 3 h p.i. were visualized by confocal microscopy. Staining was done with the rabbit anti-polyomavirus virion serum followed by the Alexa Fluor 488-goat anti-rabbit IgG antibody (green). DNA was visualized with propidium iodide (red). Bars in panels a to e, 5 μm. Bar in panel f, 2 μm.

rapidly along microtubules and deliver SV40 to syntaxin 17-positive, smooth ER (29). Our observations are, in many respects, in striking agreement with their findings: (i) the presence of caveolin on particle-containing monopinocytic vesicles which fuse frequently with caveolin-rich endosomes, heterogeneous in size and shape, (ii) alignment of VP1 and tubulin signals at later times postadsorption (3 h), (iii) the accumulation of VP1 around the nuclear membrane, very probably in the ER, and (iv) the absence of free viral particles in the cytosol. On the other hand, we occasionally observed direct fusion of monopinocytic vesicles carrying virus with the ER, and we did not find the reported long, tubular virus-containing endosomes. Moreover, the authors reported that tubular carriers do not contain caveolin, but we monitored the colocalization of polyomavirus VP1 with caveolin-1 from the plasma membrane up to perinuclear areas. Because the tubular SV40-containing carriers are dynamic structures, moving rapidly along microtubules (29), they might have eluded the detection techniques we used. The inhibition of polyomavirus infection by nocodazole was documented (18). Further studies are needed to clearly determine if caveolin is required for the productive route of polyomavirus viral particles. SV40 infection was blocked by expression of the dominant-negative mutant of caveolin (32) and was inhibited by nystatin and filipin (2). We observed strong inhibition of the infectivity of both polyomavirus and SV40 by methyl-β-cyclodextrin in concentrations that did not significantly block the uptake of transferrin.

Surprisingly, Gilbert and Benjamin (11) observed little or no colocalization of polyomavirus VP1 and caveolin in primary mouse kidney cells and NIH 3T3 fibroblasts. Moreover, they reported no effect of nystatin and filipin, as well as a clathrin-blocking agent, and also no effect of expression of a dominant-negative mutant of dynamin I (required for the formation of both caveola-derived and clathrin-coated vesicles), on polyomavirus infection.

We detected no convincing VP1 signal from incoming VP1 pseudocapsids and virions in the cell nuclei. This was a surprising finding because it had been reported that VP1 pseudocapsids (1) and virions of polyomavirus and also SV40 enter the nucleus and become uncoated quickly thereafter (6, 14, 20, 43, 44). These results suggest either that only a few entire virions enter the cell nucleus (and thus are below the detection level) and the vast majority of viral particles becomes disassembled and subsequently degraded in the cytoplasm or that the VP1 of virions entering the nucleus becomes degraded more quickly than that remaining in the cytoplasm. Masking of VP1 epitopes by nuclear proteins may be another possibility. Finally, the question of whether virion uncoating could take place on cytoplasmic or nuclear membrane structures, and only viral nucleocores would pass through nucleopores (or bypass them and enter directly through nuclear membranes), should be reconsidered. The maximum diameter of a particle that can pass through the pore is estimated at 23 nm (7, 8), while the diameter of the polyomavirus virion is about 50 nm. Experiments monitoring the localization of individual structural proteins of polyomavirus and polyomaviral DNA are under way to help solve this problem.

Despite the remarkable differences in the efficiency of DNA

delivery mediated by virions and VP1 pseudocapsids, with both electron and confocal microscopy we found no substantial differences in the movement of virions and VP1 pseudocapsids. We cannot rule out the possibility that at least some of the processes observed represent the defense of cells against viral particle invasion. On the other hand, both the inner content of particles and the absence or presence of minor structural proteins, VP2 and VP3, may account for subtle differences in molecular interactions in cells, apparently through changes in the particle surface conformation. VP1 pseudocapsids might be handicapped in the process of DNA uncoating, but the fate of viral particles may already be decided in a very early step of its adsoption on the plasma membrane, in sorting endosomes, and/or in ER compartments.

ACKNOWLEDGMENTS

This work was supported by HHMI USA grant 75195-540501, by grant 204/00/0271 from the Grant Agency of the Czech Republic, and by grant VS 96135 from the Ministry of Education of the Czech Republic.

We are grateful to Michael Pawlita and Harumi Kasamatsu for gifts of antibodies, to Jan Kovář for transferrin, and to Jiřina Hanová and Alice Křížová for assistance in preparation of the manuscript.

REFERENCES

1. **An, K., A. Q. Paulsen, M. B. Tilley, and R. A. Consigli.** 2000. Use of electron microscopic and immunogold labeling techniques to determine polyomavirus recombinant VP1 capsid-like particles entry into mouse 3T6 cell nucleus. J. Virol. Methods **90:**91–97.
2. **Anderson, H. A., Y. Chen, and L. C. Norkin.** 1996. Bound simian virus 40 translocates to caveolin-enriched membrane domains, and its entry is inhibited by drugs that selectively disrupt caveolae. Mol. Biol. Cell. **11:**1825–1834.
3. **Anderson, H. A., Y. Chen, and L. C. Norkin.** 1998. MHC class I molecules are enriched in caveolae but do not enter with simian virus 40. J. Gen. Virol. **79:**1469–1477.
4. **Atwood, W. J., and L. C. Norkin.** 1989. Class I major histocompatibility proteins as cell surface receptors for simian virus 40. J. Virol. **63:**4474–4477.
5. **Bartlett, J. S., R. Wilcher, and R. J. Samulski.** 2000. Infectious entry pathway of adeno-associated virus and adeno-associated virus vectors. J. Virol. **74:** 2777–2785.
6. **Clever, J., M. Yamada, and H. Kasamatsu.** 1991. Import of simian virus 40 virions through nuclear pore complexes. Proc. Natl. Acad. Sci. USA **88:**7333–7337.
7. **Dworetzky, S. I., and C. M. Feldherr.** 1988. Translocation of RNA-coated gold particles through the nuclear pores of oocytes. J. Cell Biol. **106:**575–584.
8. **Feldherr, C. M., E. Kallenbach, and N. Schultz.** 1984. Movement of a karyophilic protein through the nuclear pores of oocytes. J. Cell Biol. **99:** 2216–2222.
9. **Forstová, J., N. Krauzewicz, S. Wallace, A. J. Street, S. M. Dilworth, S. Beard, and B. E. Griffin.** 1993. Cooperation of structural proteins during late events in the life cycle of polyomavirus. J. Virol. **67:**1405–1413.
10. **Forstová, J., N. Krauzewicz, V. Sandig, J. Elliott, Z. Palková, M. Strauss, and B. E. Griffin.** 1995. Polyoma virus pseudocapsids as efficient carriers of heterologous DNA into mammalian cells. Hum. Gene Ther. **6:**297–306.
11. **Gilbert, J. M., and T. L. Benjamin.** 2000. Early steps of polyomavirus entry into cells. J. Virol. **74:**8582–8588.
12. **Gillock, E. T., S. Rottinghaus, D. Chang, X. Cai, S. A. Smiley, K. An, and R. A. Consigli.** 1997. Polyomavirus major capsid protein VP1 is capable of packaging cellular DNA when expressed in the baculovirus system. J. Virol. **71:**2857–2865.
13. **Griffith, G. R., and R. A. Consigli.** 1984. Isolation and characterization of monopinocytotic vesicles containing polyomavirus from the cytoplasm of infected mouse kidney cells. J. Virol. **50:**77–85.
14. **Griffith, G. R., S. J. Marriott, D. A. Rintoul, and R. A. Consigli.** 1988. Early events in polyomavirus infection: fusion of monopinocytotic vesicles containing virions with mouse kidney cell nuclei. Virus Res. **10:**41–51.
15. **Haun, G., O. T. Keppler, C. T. Bock, M. Herrmann, H. Zentgraf, and M. Pawlita.** 1993. The cell surface receptor is a major determinant restricting the host range of the B-lymphotropic papovavirus. J. Virol. **67:**7482–7492.
16. **Hink, W. F.** 1970. Established insect cell line from cabbage looper, *Trichoplusia ni*. Nature (London) **226:**466–467.
17. **Keppler, O. T., P. Stehling, M. Herrmann, H. Kayser, D. Grunow, W. Reutter, and M. Pawlita.** 1995. Biosynthetic modulation of sialic acid-dependent virus-receptor interactions of two primate polyoma viruses. J. Biol. Chem. **270:**1308–1314.
18. **Krauzewicz, N., J. Štokrová, C. Jenkins, M. Elliott, C. F. Higgins, and B. E. Griffin.** 2000. Virus-like gene transfer into cells mediated by polyoma virus pseudocapsids. Gene Ther. **7:**2122–2131.
19. **Lee, J. Y., J. A. Marshall, and D. S. Bowden.** 1994. Characterization of rubella virus replication complexes using antibodies to double-stranded RNA. Virology **200:**307–312.
20. **Mackay, R. L., and R. A. Consigli.** 1976. Early events in polyomavirus infection: attachment, penetration, and nuclear entry. J. Virol. **19:**620–636.
21. **Michaely, P. A., C. Mineo, Y. S. Ying, and R. G. Anderson.** 1999. Polarized distribution of endogenous Rac1 and RhoA at the cell surface. J. Biol. Chem. **274:**21430–21436.
22. **Montross, L., S. Watkins, R. B. Moreland, H. Mamon, D. L. Caspar, and R. L. Garcea.** 1991. Nuclear assembly of polyomavirus capsids in insect cells expressing the major capsid protein VP1. J. Virol. **65:**4991–4998.
23. **Moreland, R. B., L. Montross, and R. L. Garcea.** 1991. Characterization of the DNA-binding properties of the polyomavirus capsid protein VP1. J. Virol. **65:**1168–1176.
24. **Norkin, L. C.** 1999. Simian virus 40 infection via MHC class I molecules and caveolae. Immunol. Rev. **168:**13–22.
25. **Palková, Z., T. Adamec, D. Liebl, J. Štokrová, and J. Forstová.** 2000. Production of polyomavirus structural protein VP1 in yeast cells and its interaction with cell structures. FEBS Lett. **478:**281–289.
26. **Parton, R. G., and M. Lindsay.** 1999. Exploitation of major histocompatibility complex class I molecules and caveolae by simian virus 40. Immunol. Rev. **168:**23–31.
27. **Patterson, S., and W. C. Russell.** 1983. Ultrastructural and immunofluorescence studies of early events in adenovirus-HeLa cell interactions. J. Gen. Virol. **64:**1091–1099.
28. **Pawlita, M., M. Muller, M. Oppenlander, H. Zentgraf, and M. Herrmann.** 1996. DNA encapsidation by virus-like particles assembled in insect cells from the major capsid protein VP1 of B-lymphotropic papovavirus. J. Virol. **70:**7517–7526.
29. **Pelkmans, L., J. Kartenbeck, and A. Helenius.** 2001. Caveolar endocytosis of simian virus 40 reveals a new two step vesicular-transport pathway to the ER, Nat. Cell Biol. **3:**473–483.
30. **Pho, M. T., A. Ashok, and W. J. Atwood.** 2000. JC virus enters human glial cells by clathrin-dependent receptor-mediated endocytosis. J. Virol. **74:**2288–2292.
31. **Rando, O. J., K. Zhao, and G. R. Crabtree.** 2000. Searching for a function for nuclear actin. Trends Cell Biol. **10:**92–97.
32. **Roy, S., R. Luetterforst, A. Harding, A. Apolloni, M. Etheridge, E. Stang, B. Rolls, J. F. Hancock, and R. G. Parton.** 1999. Dominant-negative caveolin inhibits H-Ras function by disrupting cholesterol-rich plasma membrane domains. Nat. Cell Biol. **2:**98–105.
33. **Shimura, H., Y. Umeno, and G. Kimura.** 1987. Effects of inhibitors of the cytoplasmic structures and functions on the early phase of infection of cultured cells with simian virus 40. Virology **158:**34–43.
34. **Simons, K., and D. Toomre.** 2000. Lipid rafts and signal transduction. Nat. Rev. **1:**31–39.
35. **Simons, K., and E. Ikonen.** 1997. Functional rafts in cell membranes. Nature **387:**569–572.
36. **Soeda, E., N. Krauzewicz, C. Cox, J. Štokrová, J. Forstová, and B. E. Griffin.** 1998. Enhancement by polylysine of transient, but not stable, expression of genes carried into cells by polyoma VP1 pseudocapsids. Gene Ther. **5:**1410–1419.
37. **Stehle, T., S. J. Gamblin, Y. Yan, and S. C. Harrison.** 1996. The structure of simian virus 40 refined at 3.1 Ĺ resolution. Structure **4:**165–182.
38. **Štokrová, J., Z. Palková, L. Fischer, Z. Richterová, J. Korb, B. E. Griffin, and J. Forstová.** 1999. Interactions of heterologous DNA with polyomavirus major structural protein, VP1. FEBS Lett. **445:**119–125.
39. **Summers, M. D., and G. E. Smith.** 1987. A manual of methods for baculovirus vectors and insect culture procedures. Texas Agricultural Experiment Station, bulletin no. 1555. Texas A&M University, College Station, Tex.
40. **Türler, H., and P. Beard.** 1985. Simian virus 40 and polyomavirus: growth, titration, transformation and purification of viral components, p. 169–192. *In* B. W. J. Mahz (ed.), Virology: a practical approach. IRL Press, Oxford, United Kingdom..
41. **Varga, M. J., C. Weibull, and E. Everitt.** 1991. Infectious entry pathway of adenovirus type 2. J. Virol. **65:**6061–6070.
42. **Whittaker, G. R., M. Kann, and A. Helenius.** 2000. Viral entry into the nucleus. Annu. Rev. Cell Dev. Biol. **16:**627–651.
43. **Winston, V. D., J. B. Bolen, and R. A. Consigli.** 1980. Isolation and characterization of polyoma uncoating intermediates from the nuclei of infected mouse cells. J. Virol. **33:**1173–1181.
44. **Yamada, M., and H. Kasamatsu.** 1993. Role of nuclear pore complex in simian virus 40 nuclear targeting. J. Virol. **67:**119–130.
45. **Zhou, J., L. Gissmann, H. Zentgraf, H. Muller, M. Picken, and M. Muller.** 1995. Early phase in the infection of cultured cells with papillomavirus virions. Virology **214:**167–176.
46. **Zullo, J., C. D. Stiles, and R. L. Garcea.** 1987. Regulation of c-*myc* and c-*fos* mRNA levels by polyomavirus: distinct roles for the capsid protein VP1 and the viral early proteins. Proc. Natl. Acad. Sci. USA **84:**1210–1214.